Eur. Phys. J. D **14**, 77–81 (2001)

THE EUROPEAN PHYSICAL JOURNAL D

EDP Sciences

Magnetic Thomas-Fermi-Weizsäcker model for quantum dots: A comparison with Kohn-Sham ground states

Ll. Serra[a] and A. Puente

Departament de Física, Universitat de les Illes Balears, 07071 Palma de Mallorca, Spain

Received 26 October 2000 and Received in final form 14 December 2000

Abstract. The magnetic extension of the Thomas-Fermi-Weizsäcker kinetic energy is used within density-functional-theory to numerically obtain the ground state densities and energies of two-dimensional quantum dots. The results are thoroughly compared with the microscopic Kohn-Sham ones in order to assess the validity of the semiclassical method. Circular as well as deformed systems are considered.

PACS. 73.20.Dx Electron states in low-dimensional structures (superlattices, quantum well structures and multilayers) – 78.20.Bh Theory, models and numerical simulation

1 Introduction

Semiclassical approaches to many-body systems are a very valuable tool since they provide physical insights which otherwise are very difficult to achieve. In fact, they have been applied since many years ago to describe different systems such as atoms, atomic nuclei, metals and, more recently, metallic clusters and electronic nanostructures. Two dimensional quantum dots are not an exception and have been analyzed using the Thomas-Fermi models in, for instance, references [1–6].

In reference [7] we performed calculations for quantum dots using a selfconsistent Thomas-Fermi-Weizsäcker (TFW) model similar to that developed by Zaremba and coworkers [5]. It is our aim in this paper to extend those calculations by including the effect of a perpendicular magnetic field B using the magnetic extension of the kinetic energy within density-functional theory. As in reference [7] we will pay special attention to the quantitative comparison with the microscopic Kohn-Sham solution in order to asses the accuracy limits of the TFW densities and energies as a function of B. The magnetic extension of the Thomas-Fermi theory was rigorously presented by Lieb *et al.* [3] and a selfconsistent numerical application to circular dots was done in reference [4] but, to our knowledge, no detailed comparison with microscopic calculations has been given in the literature. We also present in this manuscript symmetry unrestricted calculations for deformed dots that had not been considered before within this model.

A peculiar characteristic of the magnetic Thomas-Fermi functional is its first-derivative discontinuity in the density dependence [3], at particular density values. The physical origin for this is found in the formation of constant energy Landau-bands in the non-interacting Fermi gas at certain magnetic fields. This implies that the mean field is discontinuous, thus manifesting the formation of *incompressible regions* in the system, each one characterized by the number of full Landau bands, *i.e.*, the filling factor ν. It is worth to point out that experimental evidences of incompressible stripes at the edges of quantum dots and antidots have been obtained by means of far-infrared spectroscopy [8]. As we will show, the semiclassical Euler-Lagrange equations selfconsistently determine the density profile, energy and chemical potential of the quantum dot, which turn out to be in an overall good agreement with full Kohn-Sham results for increasing magnetic fields up to $\nu = 1$.

Section 2 of the paper is devoted to the presentation of the energy functional as well as the minimization equations. In Section 3 the results for circular as well as deformed quantum dots are given and, finally, Section 4 presents the conclusions.

2 Magnetic TFW functional

Using a local approximation to density functional theory we assume that the energy of the system can be written in terms of the electronic spin densities $\rho_\eta(\mathbf{r})$, where $\eta = \uparrow, \downarrow$, as $E = \int \mathrm{d}\mathbf{r}\mathcal{E}[\rho_\uparrow, \rho_\downarrow; B]$. Notice also the explicit dependence on the magnetic field B which is considered as a functional parameter. The different contributions to the energy density may be written as

$$\mathcal{E}[\rho_\uparrow, \rho_\downarrow; B] = \tau[\rho_\uparrow; B] + \tau[\rho_\downarrow; B] + \frac{1}{2}v_{\mathrm{H}}(\mathbf{r})\rho + \mathcal{E}_{\mathrm{XC}}(\rho_\uparrow, \rho_\downarrow) + v_{\mathrm{ext}}(\mathbf{r})\rho + \mathcal{E}_{\mathrm{Z}}(\rho_\uparrow, \rho_\downarrow; B), \quad (1)$$

where the first two pieces give the kinetic energies of spin up and down electrons; the third is the Hartree energy in

[a] e-mail: dfslsc4@clust.uib.es

terms of the Hartree potential $v_{\rm H}$ and the total density $\rho = \rho_\uparrow + \rho_\downarrow$; the fourth is the exchange-correlation contribution; the fifth is the energy due to the external potential $v_{\rm ext}$ and, the last one corresponds to the Zeeman contribution. As in references [5,7], the kinetic energy contains a pure Thomas-Fermi term and a gradient (Weizsäcker) one, $\tau = \tau_{\rm TF} + \tau_{\rm W}$. The gradient term is given by

$$\tau_{\rm W}[\rho_\eta] = \frac{\hbar^2}{2m}\lambda\frac{(\nabla\rho_\eta)^2}{\rho_\eta}, \tag{2}$$

with $\lambda = 1/4$, while the Thomas-Fermi piece is [3,4]

$$\tau_{\rm TF}[\rho_\eta; B] = \frac{1}{2}\hbar\omega_{\rm c} D S_\eta^2 + \hbar\omega_{\rm c}\left(S_\eta + \frac{1}{2}\right)(\rho_\eta - S_\eta D)\,. \tag{3}$$

In this last expression $\omega_{\rm c} = eB/mc$ is the cyclotron frequency, $D = eB/2\pi\hbar c$ is the Landau level degeneracy per unit area and $S_\eta = [\rho_\eta/D]$ is the integer part [9] of the local filling factor $\nu_\eta = \rho_\eta/D$ and gives the index of the highest fully occupied Landau band. The two contributions in equation (3) give therefore the kinetic energy of the fully occupied Landau bands and that corresponding to the last partially filled band, respectively. It can be shown [3] that, in the limit $B \to 0$, the non-magnetic Thomas-Fermi functional $\tau_{\rm TF}(\rho, B = 0) = \hbar^2\pi\rho^2/2m$ is recovered from equation (3).

For the exchange-correlation energy $\mathcal{E}_{\rm XC}$ we have used the LSDA functional based on the Tanatar-Ceperley calculations for the 2D uniform electron gas [10] and the von Barth-Hedin interpolation for intermediate polarizations [11]. The expression can be found, *e.g.*, in reference [12], where Kohn-Sham results for parabolic dots at $B = 0$ were given. Notice that current-density dependence is not included in the functional. This could in principle be done within the so-called current-density-functional theory although it is known that the contribution to the ground state energy from these terms is in general quite small and only at very high magnetic fields they can be of relevance [13,14].

The Zeeman energy reads, in terms of the effective gyromagnetic factor g^* and Bohr magneton $\mu_{\rm B}$,

$$\mathcal{E}_{\rm Z}(\rho_\uparrow, \rho_\downarrow; B) = \frac{1}{2}g^*\mu_{\rm B}B(\rho_\uparrow - \rho_\downarrow). \tag{4}$$

The energy functional is minimized by the ground state spin densities, or equivalently by the ground state total density ρ and magnetization $m = \rho_\uparrow - \rho_\downarrow$, with the constraint of conservation of the total number of particles. The corresponding Lagrange parameter μ is, by definition, the chemical potential. The two sets of equivalent equations read

$$\begin{cases} \dfrac{\delta E}{\delta\rho} = \mu \\ \dfrac{\delta E}{\delta m} = 0 \end{cases} \quad \Leftrightarrow \quad \begin{cases} \dfrac{\delta E}{\delta\rho_\uparrow} = \mu \\ \dfrac{\delta E}{\delta\rho_\downarrow} = \mu \end{cases}. \tag{5}$$

For convenience, we choose to work with the second set which can be transformed, introducing new variables $\psi_\eta = \sqrt{\rho_\eta}$, into the alternative Schrödinger-like equations

$$-4\lambda\frac{\hbar^2}{2m}\nabla^2\psi_\eta + \left(v_{\rm ext} + v_{\rm H} + \frac{\partial\mathcal{E}_{\rm XC}}{\partial\rho_\eta} + C_\eta + \alpha_\eta\frac{g^*}{2}\mu_{\rm B}B\right)\psi_\eta = \mu\psi_\eta, \tag{6}$$

where we have defined $\alpha_\uparrow = 1$, $\alpha_\downarrow = -1$ and also introduced the contribution from the Thomas-Fermi energy

$$C_\eta = \hbar\omega_{\rm c}\left(S_\eta + \frac{1}{2}\right). \tag{7}$$

The solution of the two coupled equations (6), *i.e.*, for each spin component, has been obtained numerically by discretizing the two-dimensional xy-plane into a uniform grid of points and using the imaginary time-step method. The grid size is typically 70×70 points, while the Laplacian operator is discretized by using 7 points formulas. The stability of the results when increasing these values has been checked. The Kohn-Sham results, we will compare with below, have been obtained using a similar method developed by us in reference [15].

3 Results

3.1 The TF plateaus

We begin the results section by discussing the effect of the discontinuous contribution to the potential. We present here calculations for two different dots: a circular one containing $N = 42$ electrons under parabolic confinement $v_{\rm ext} = (1/2)\omega_0^2 r^2$ [16,17] and a second one containing $N = 20$ electrons in a deformed parabola

$$v_{\rm ext}(\mathbf{r}) = \frac{1}{2}\omega_0^2\frac{4}{(1+\beta)^2}(x^2 + \beta^2 y^2), \tag{8}$$

with anisotropy factor [18] $\beta = 0.75$ and a coefficient ω_0 given by $N_{\rm p} = 20$ and the same $r_{\rm s}$ as for $N = 42$.

The spin up and down densities for the circular dot are displayed in the upper-left panel of Figure 1, in comparison with the corresponding Kohn-Sham ones. The horizontal dotted lines indicate the values $\rho = D$ and $2D$ where D is the density for bulk filling factor $\nu = 1$ (Sect. 2). The TFW density is clearly giving flat regions, *i.e.*, plateaus, at the densities of the bulk integer filling factors, which must be associated with incompressible stripes in the finite system. Due to the effect of the Weizsäcker term the transition between different plateaus is quite smooth. In this particular case the spin down density has attained the first plateau and is beginning to fill a second one around the dot center. On the other hand, the spin up density has already reached the second plateau at the center of the dot.

The correlation of the plateaus with Landau bands is made even clearer in the upper-right panel, where the

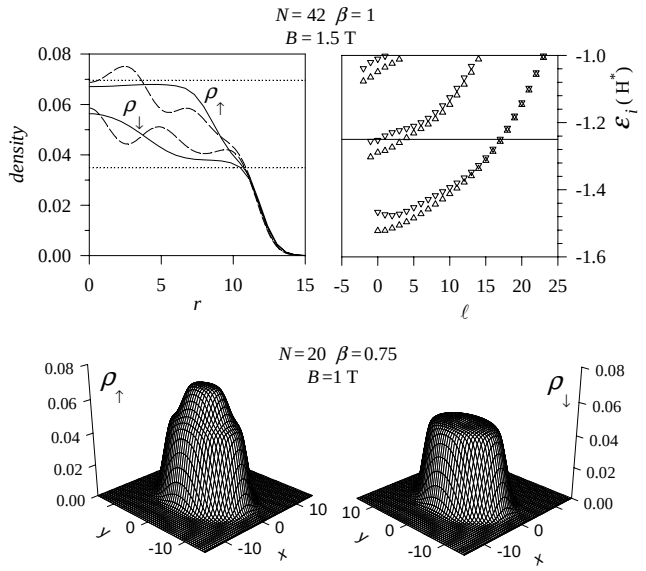

Fig. 1. Upper row: left panel shows spin up and down densities with TFW (solid) and Kohn-Sham (dashed) models. Dotted lines indicate the bulk densities for filling factor 1 and 2. Right panel displays the (spin up/down) KS eigenvalues (up/down triangles) as a function of orbital angular momentum. The horizontal line indicates the Fermi energy (effective atomic units [16] are used). Lower row: spin densities for a deformed quantum dot (see Sect. 3).

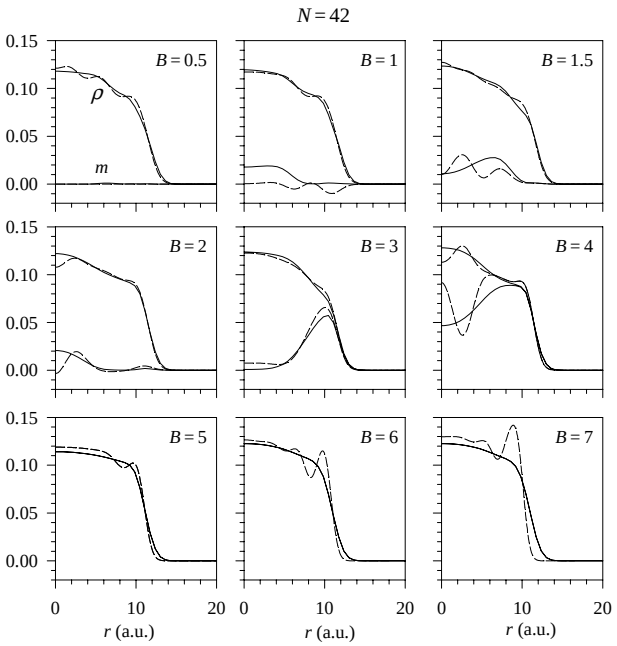

Fig. 2. Evolution with magnetic field of density $\rho(r)$ and magnetization $m(r)$ for the circular dot with $N = 42$. Solid lines correspond to TFW and dashed ones to KS. In each panel the curves with lower values at the origin correspond to $m(r)$, except for $B > 4$ T where the dot is fully polarized and thus $m = \rho$.

Kohn-Sham eigenvalues are plotted as a function of orbital angular momentum ℓ. In this plot the horizontal line at $\epsilon \approx -1.24H^*$ indicates the Fermi energy. A proportionality between ℓ and r may be established by noting that high ℓ values imply outer orbits. Therefore, at the dot center (low ℓ's) two spin up bands are filled while for spin down the second band is only partly occupied. When going towards the edge (increasing ℓ) the second spin down band is rapidly depleted and at a larger r the same happens with the second spin up band. This behaviour of the microscopic solution is in excellent agreement with that inferred from the plateaus of the left panel, thereby showing the quality of the model. The formation of the plateaus is not as clear in the KS densities because of rather large density oscillations, quite similar to the Friedel oscillations found in metals.

The two lower plots of Figure 1 show the plateaus in spin up and down densities for the deformed dot at $B = 1$ T. A behaviour similar to that of the circular case is inferred, although in this case the plateaus adjust their shape to the anisotropy $\beta = 0.75$ of the confining potential. At larger magnetic fields, however, deviations are obtained as we will show when presenting the systematic results in Section 3.3

3.2 Circular dot with 42 electrons

In this subsection we show in a systematic way the results for the dot containing $N = 42$ electrons in a circular parabola, with $r_s = 1.5a_0^*$ and $N_p = 42$. Figure 2 displays the evolution with magnetic field of the density and magnetization profiles in comparison with the Kohn-Sham ones. In general the TFW density and magnetization are correctly averaging the KS values with a rather good agreement for all the magnetic fields considered. At $B = 5$ T the TFW correctly yields equal density and magnetization distributions, due to the achievement of full polarization. At this magnetic field the KS result corresponds to the maximum-density-droplet (MDD) solution [19], in which the single-particle angular momenta are successively occupied up to the $\ell_{max} = N-1$ value. Increasing the magnetic field still further, *i.e.*, entering the region of fractional filling factor $\nu < 1$, the dot evolves by reconstructing the edge, as seen in the $B = 6$ and 7 T panels. However, this physical behaviour is apparently not well reproduced by the TFW model.

In the upper-left panel of Figure 3 a quantitative comparison between the energy per particle in TFW and KS is provided. We see that the difference remains below 2%, although on the plot it may seem magnified because of the expanded scale. In the upper-right panel a comparison of the TFW chemical potential μ with the KS Fermi energy is given, which is again indicating the good estimate given by the TFW of the less bound electron, until the edge reconstruction begins. We mention that we remain here in the limit $T \to 0$, although a small value of T is sometimes necessary to converge the KS results.

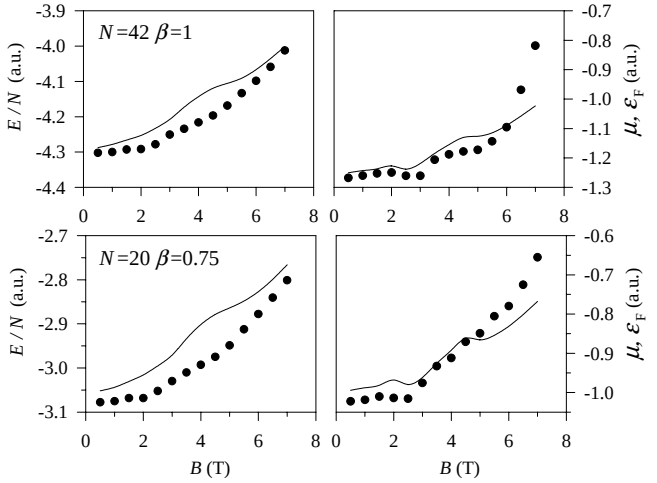

Fig. 3. Upper panels: (left) energy per particle within the TFW (solid) and KS (dots) models; (right) TFW chemical potential (solid) *vs.* KS Fermi energy (dots) for the circular system with $N = 42$ electrons. Lower panels: corresponding values for $N = 20$ electrons in a deformed parabola.

3.3 Elliptic dot with N = 20

The lower panels in Figure 3 represent the comparison of the ground state energy per particle E/N and TFW chemical potential *vs.* KS Fermi energy corresponding to the 20-electron dot in a deformed parabola (Sect. 3.1). As for the previous circular system the agreement between the TFW and KS ground state energies is remarkable, not exceeding in this case a 3%.

Figures 4 and 5 show within TFW and KS, respectively, the local filling factors ν for selected values of the magnetic field. A similar behaviour as that discussed for the circular case is obtained. In fact we recognize the preference of the TFW density to produce flat regions associated with the integer filling factors. By looking at the central region we can also identify the progressive depletion of the central plateau when increasing the magnetic field. For instance, one can follow the evolution $\nu = 3, 2, 1$ for $B = 1, 1.5, 2.5$ T, respectively. This behavior is also inferred from the KS results (Fig. 5) although it is somehow masked by the large oscillations of quantum origin. As in the circular case, the prediction of the dot polarization with magnetic field is also in good agreement with the microscopic result. This can be qualitatively seen in Figures 4 and 5 by noting the clear depletion of the spin down density starting at $B = 3$ T which ends with a fully polarized dot ($S = 10$) for $B \geq 4.5$ T.

A conspicuous prediction of the KS model is the gradual change in shape of the quantum dot when increasing the magnetic field. This is quite evident for $B \geq 4$ T, when the dot can no longer be considered elliptic, but rather rectangular in shape. We attribute this to the competition between the symmetry of the external field and the preference for circular edge reconstructions induced by large magnetic fields. A more abrupt transition to a circular shape was obtained in reference [20] within the ultimate jellium model, which permits the deformation of the external potential. In our model this is fixed and, therefore, it seems natural that a stronger competition is present. When comparing with the TFW results, we notice that although the central plateau indeed seems to evolve towards a rectangle (for $B = 4.5{-}5.5$ T), the outer edge remains always elliptic. The deficiency of the semiclassical model in reproducing morphological changes attributed to the magnetic field can be explained by the fact that within TFW the magnetic field effects are taken into account in a purely local way (see Eq. (7)), and thus can hardly induce any influence on the global shape. Another missing feature in the TFW results is the incipient electron localization seen in the KS panels for $B > 6$ T (Fig. 5). This localization has also been predicted within Hartree-Fock theory [21] and more recently, using current-density-functional theory [14].

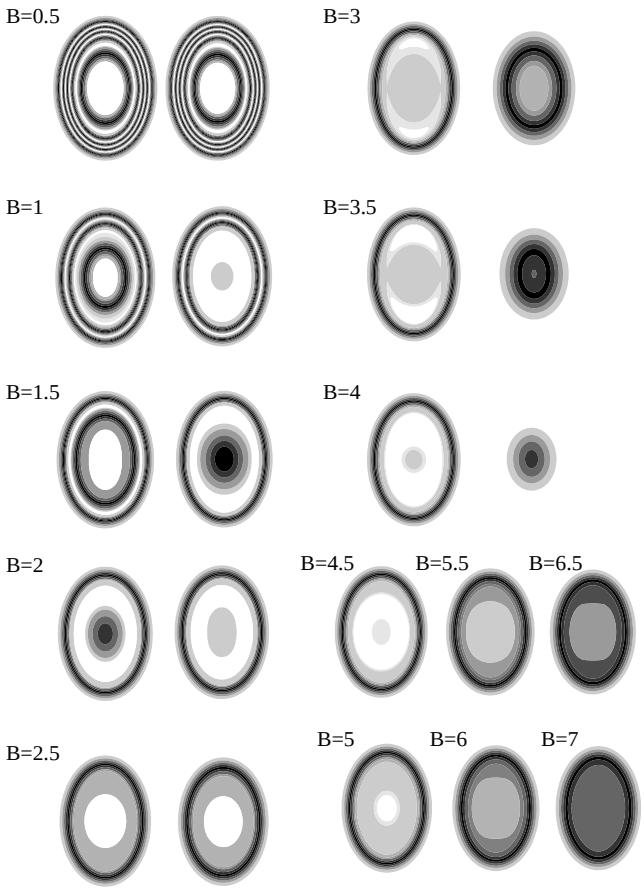

Fig. 4. Evolution, within the TFW model, of the local filling factor with magnetic field for the elliptic dot with $N = 20$ electrons. In each case spin up (left) and down (right) values are shown, except for $B \geq 4.5$ T in which only the spin up result is represented since full polarization has been attained. White areas correspond to near-integer values (plateaus) while black contours indicate half-integer transition values.

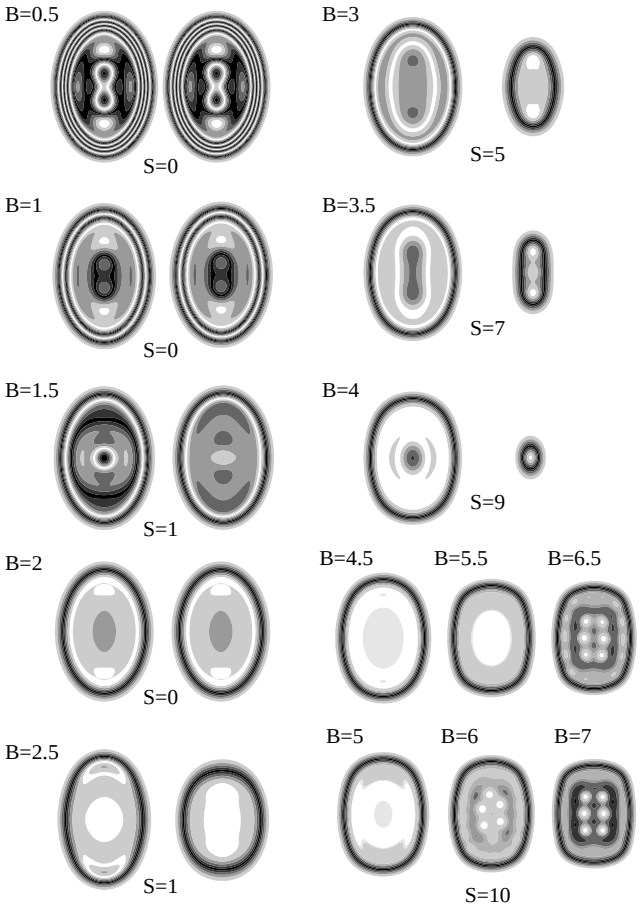

Fig. 5. Same as Figure 4 within KS. The ground state total spin is indicated at the bottom of the plot for each magnetic field. For $B \geq 4.5$ T, the dot is fully polarized and thus $S = 10$.

4 Conclusions

The validity limits of the semiclassical TFW model have been discussed by comparing with the microscopic Kohn-Sham model. The magnetic extension of the semiclassical kinetic energy produces a discontinuous mean field which favours the appearance of density plateaus corresponding to integer filling factors for the bulk gas. The correspondence of these plateaus with the occupation of Landau bands in the finite systems has been proved for a circular dot with $N = 42$ electrons. In circular dots, the systematic evolution with B of the density and magnetization profiles is rather well predicted by the TFW model up to filling factor $\nu = 1$. The same happens with the dot energy and chemical potential. In deformed dots the ground state energy is also well reproduced by TFW, although this model is not able to yield the shape changes induced by the magnetic field, as found in the KS result.

This work has been performed under Grant No. PB98-0124 from DGESeIC, Spain.

References

1. P.L. McEuen, E.B. Foxman, J. Kinaret, U. Meirav, M.A. Kastner, N.S. Windgreen, S.J. Wind, Phys. Rev. B **45**, 11419 (1992).
2. I.K. Marmokos, C.W. Beenaker, Phys. Rev. B **46**, 15562 (1992).
3. E.H. Lieb, J.P. Solovej, J. Ingvason, Phys. Rev. B **51**, 10646 (1995).
4. N. Barberan, Phys. Rev. B **58**, 12970 (1998).
5. E. Zaremba, Phys. Rev. B **53**, 10512 (1996); E. Zaremba, H.C. Tso, Phys. Rev. B **49**, 8147 (1994); B.P. van Zyl, E. Zaremba, D.A.W. Hutchinson, Phys. Rev. B **61**, 2107 (2000).
6. R. Pino, Eur. Phys. J. B **13**, 723 (2000).
7. A. Puente, M. Casas, Ll. Serra, Physica E **8**, 387 (2000).
8. K. Bollweg *et al.*, Phys. Rev. Lett. **76**, 2774 (1996); see also comment, T. Darnhoffer, M. Suhrke, U. Rössler, Phys. Rev. Lett. **77**, 2593 (1996); reply, Bollweg *et al.*, Phys. Rev. Lett. **77**, 2594 (1996).
9. For computational stability the integer-part function $[x]$ is smoothed in the following way $[x] \approx \sum_{i=1}[1 + \tanh((x-i)/\lambda)]/2$ with $\lambda = 0.05a_0^*$. For λ small enough the results are not sensitive on its precise value.
10. B. Tanatar, D.M. Ceperley, Phys. Rev. B **39**, 5005 (1989).
11. U. von Barth, L. Hedin, J. Phys. C **5**, 1629 (1972).
12. M. Koskinen, M. Manninen, S.M. Reimann, Phys. Rev. Lett. **79**, 1389 (1997).
13. M. Ferconi, G. Vignale, Phys. Rev. B **50**, 14722 (1994).
14. S.M. Reimann *et al.*, Phys. Rev. Lett. **83**, 3270 (1999).
15. A. Puente, Ll. Serra, Phys. Rev. Lett. **83**, 3266 (1999).
16. We use the standard effective units system, defined by $\hbar = e^2/\epsilon = m = 1$, where ϵ is the dielectric constant and m is the effective electron mass (given in terms of the bare mass m_e as $m = m^* m_e$). Accordingly, the length unit is given by the effective Bohr radius $a_0^* = \hbar^2\epsilon/me^2$ and the energy unit by the effective Hartree $H^* = e^2/(2\epsilon a_0^*)$. Taking the GaAs values $\epsilon = 12.4$ and $m^* = 0.067$ we get $H^* \approx 12$ meV and $a_0^* \approx 98$ Å.
17. The parabola constant is determined by $\omega_0^2 = 1/(\sqrt{N_p} r_s^3)$, with $N_p = 42$ and $r_s = 1.5a_0^*$ This definition of ω_0 is used in order to reproduce the curvature at the origin of the potential of a jellium disk containing N_p positive charges and a radius per unit charge given by r_s.
18. We define the anisotropy factor $\beta = \omega_y/\omega_x$ and the average parameter $\omega_0 = (\omega_x + \omega_y)/2$ by rewriting the confining potential as $v_{ext}(\mathbf{r}) = (\omega_x^2 x^2 + \omega_y^2 y^2)/2$.
19. A.H. McDonald, S.R.E. Yang, M.D. Johnson, Aust. J. Phys. **46**, 345 (1993).
20. S.M. Reimann, M. Koskinen, J. Kolehmainen, M. Manninen, D.G. Austing, S. Tarucha, Eur. Phys. J. D **9**, 105 (1999).
21. H.-M. Müller, S.E. Koonin, Phys. Rev. B **54**, 14532 (1996).